Icarus 354 (2021) 114046

Contents lists available at ScienceDirect

Icarus

journal homepage: www.elsevier.com/locate/icarus

# Absolute model age of lunar Finsen crater and geologic implications

Sheng Gou [a,b], Zongyu Yue [b,c], Kaichang Di [b,c,*], Zhanchuan Cai [a], Zhaoqin Liu [b], Shengli Niu [a]

[a] State Key Laboratory of Lunar and Planetary Sciences, Macau University of Science and Technology, Macau, China
[b] State Key Laboratory of Remote Sensing Science, Aerospace Information Research Institute, Chinese Academy of Sciences, Beijing 100101, China
[c] Center for Excellence in Comparative Planetology, Chinese Academy of Sciences, Hefei 230026, China

ARTICLE INFO

*Keywords:*
Finsen crater
Absolute model age
Chang'e-4 landing site
Regolith growth rate
Crater degradation/infilling rate

ABSTRACT

As the primary source of materials measured inside of Von Kármán crater by the Chang'e-4 rover, the absolute model age (AMA) of Finsen crater is derived by the crater size-frequency distribution (CSFD) measurements. Both cumulative and differential fits reveal an AMA of ~3.5 Ga, indicating Finsen crater is Imbrium-aged. Based on thickness estimation of the Finsen crater ejecta-sourced fine-grained regolith at Chang'e-4 landing site (~12 m) (Lai et al., 2019; Li et al., 2020), the average regolith growth rate at the landing site is estimated to be about 3.4 m/Gyr. The current depths of 25 largest craters on the floor of Finsen crater are calculated by the profile-average-depth method, and their original depths are estimated under the assumption that the initial depth-to-diameter (d/D) ratio is 0.2. Depth differences between current and estimated original depths, together with the AMA of Finsen crater, derive the average crater degradation/infilling rate within Finsen crater is about 21 ± 3 m/Gyr.

## 1. Introduction

China's Chang'e-4 probe, including a lander and a rover, successfully touched down within the 185-km-wide Von Kármán crater inside the South Pole-Aitken (SPA) basin on January 3, 2019, making the first-ever soft landing on the lunar farside (Di et al., 2019a) (Fig. 1). The rover Yutu-2 was released from the lander and started surface exploration on the same day. As of July 27, 2020, the rover had already operated for 20 lunar days and traversed about 490.9 m, making it the longest-working rover on the lunar surface in human history that continues to set the record. The Chang'e-4 rover has conducted a series of in situ measurements along traverse with the equipped scientific payloads: the Panoramic Camera (Pancam), the Visible and Near-Infrared Imaging Spectrometer (VNIS), and the Lunar Penetrating Radar (LPR) (Jia et al., 2018). The measured datasets enable scientists to study the unexplored area in more detail. LPR radargrams indicate that the stratigraphy of shallow subsurface structure at the landing area can be roughly divided into three units (Lai et al., 2019; Li et al., 2020): a shallower unit consisting of fine-grained regolith (depth interval, 0 to 12 m), a underlying unit consisting of coarser materials with embedded rocks (12 to 24 m), and a bottom unit containing alternating layers of coarse and fine materials (24 to 40 m). Pancam images demonstrate that surface regolith measured by the rover are lunar deep materials excavated mainly by Finsen crater (northeast of Von Kármán) with possible contributions from Alder crater (southeast of Von Kármán), and numerical simulations predict ~32 and ~35 m ejecta deposited at the landing site from Finsen and Alder, respectively (Di et al., 2019b). VNIS spectra reveal the regolith at the landing site is mature (Gou et al., 2020a), and has a forsteritic olivine and Mg-rich orthopyroxene assemblage in almost equal fractions (Gou et al., 2019; Gou et al., 2020b; Gou et al., 2020c).

As primary source of Chang'e-4 rover measured materials (e.g., Gou et al., 2019; Di et al., 2019b; Gou et al., 2020b), the formation time of Finsen crater is still unclear. A geologic map of the lunar central farside originally created in the 1970s interpreted Finsen crater as an Eratoshenian-aged crater (Stuart-Alexander, 1978; Fortezzo et al., 2020). Recently compiled geologic map of the northern portion of the SPA basin registered Finsen crater as an Imbrium-aged crater (Ivanov et al., 2018). Determination of the absolute model age (AMA) of Finsen crater as accurate as possible is of great importance for understanding the evolution of regolith at landing site. For example, the estimated fine-grained regolith thickness at the Chang'e-4 landing site is about 12 m (Lai et al., 2019; Li et al., 2020), if Finsen crater formed in the Eratosthenian period (range from about 3.2 to 1.1 billion years), the regolith formation rate should be between 3.8 m/Gyr and 10.9 m/Gyr. In this scenario, this rather high value would challenge our current knowledge on the regolith formation rate, or otherwise would indicate the lunar farside is different. The AMA of the Finsen crater is derived by the crater size-frequency distribution (CSFD) measurements in this study to

* Corresponding author at: P.O. Box 9718, No. 20A, Datun Road, Chaoyang District, Beijing, 100101, China.
*E-mail address:* dikc@radi.ac.cn (K. Di).

https://doi.org/10.1016/j.icarus.2020.114046
Received 26 April 2020; Received in revised form 31 July 2020; Accepted 1 August 2020
Available online 14 August 2020

conduct a comprehensive analysis, including regolith growth rate at Chang'e-4 landing site and crater degradation/infilling rate within Finsen crater.

## 2. Data and context

A digital orthophoto map (DOM) mosaic and a digital elevation model (DEM) mosaic generated from images collected by Chang'e-2 mission (Ren et al., 2014) are used as base maps in this study. Chang'e-2 was China's second probe to orbit the Moon, whose main objective was to image the entire lunar surface with a resolution of 7 m/pixel, to provide high resolution imagery (1.5 m /pixel) of possible landing site (Sinus Iridum) for future Chang'e-3 mission, and to test some crucial techniques for the follow-up lunar and deep space explorations (Zhao et al., 2011). The returned images were processed with radiometric, photometric, and geometric calibrations, to produce a global DOM product with a resolution of 7 m/pixel and a global DEM product with a grid spacing of 20 m using photogrammetric techniques (Ren et al., 2014). Each product is divided into 844 map subdivisions, which are stored in the Data Release and Information Service System of China's Lunar Exploration Program (http://moon.bao.ac.cn) (Ren et al., 2014). Both DOM and DEM map subdivisions that have a full coverage over the Chang'e-4 landing site and its surroundings were downloaded and mosaicked in this study for crater identification and crater depth measurement.

The location of the Chang'e-4 lander was determined to be 177.588° E, 45.457° S using visual localization techniques (Di et al., 2019a). Finsen crater (42.29° S, 177.72° W, D = 73 km), located about 135 km northeast of Chang'e-4 landing site (Fig. 1), is a well-preserved complex crater that has a prominent central peak. Representative spectra from both the central peak and crater floor exhibit similar and clear mafic absorptions, indicating the presence of low-Ca pyroxene (Moriarty et al.,

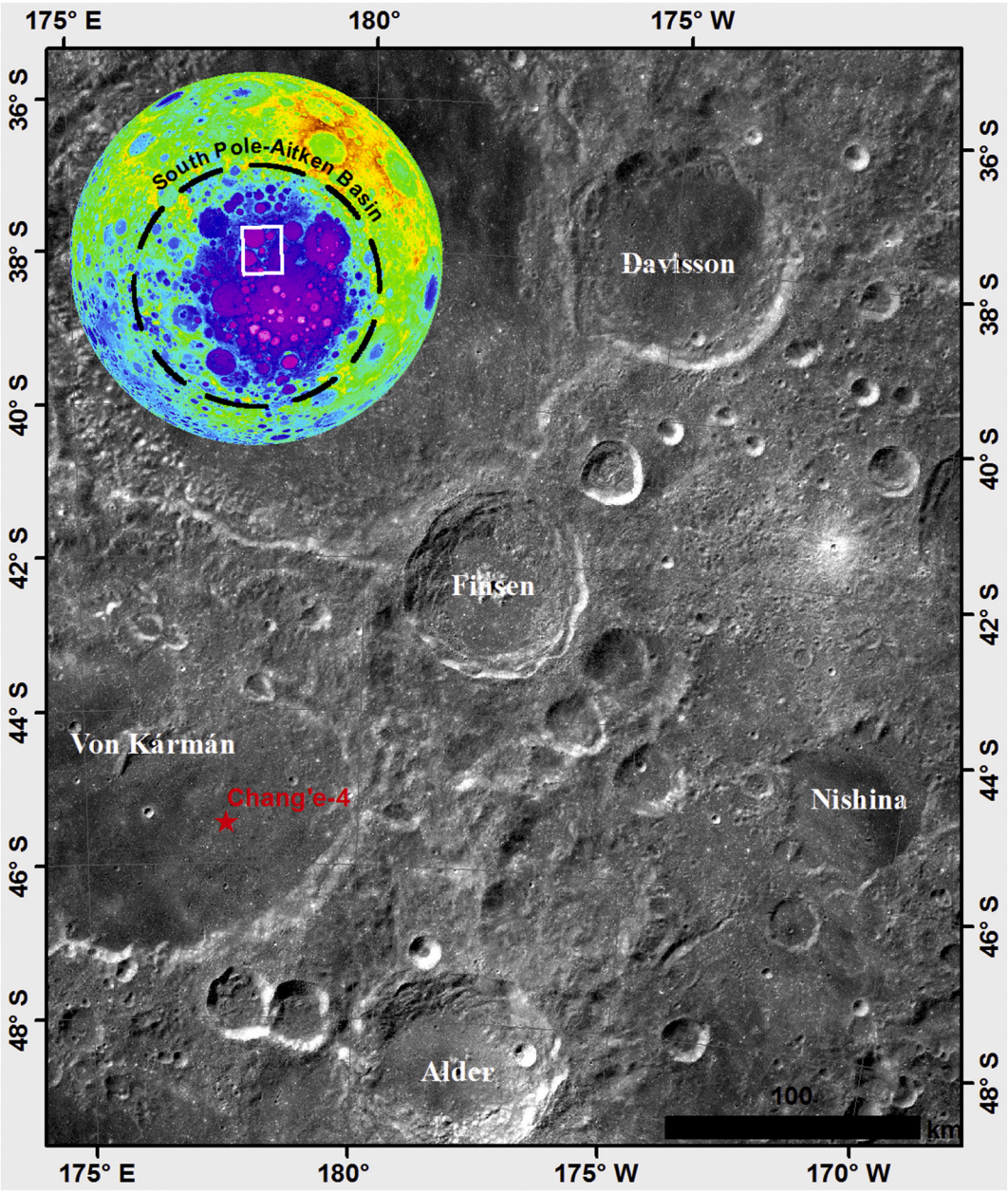


**Fig. 1.** Context map of Chang'e-4 landing site. The basemap is Chang'e-2 image mosaic (Ren et al., 2014). The Lunar Orbiter Laser Altimeter (LOLA) elevation (Smith et al., 2010) inset shows topography within the SPA basin. Colors represent different heights in the inset, with red being the highest and purple being the lowest. The white box frames the extent of Fig. 1. (For interpretation of the references to colour in this figure legend, the reader is referred to the web version of this article).

2011). Further spectral analysis revealed the pyroxene composition differs significantly from mare basalt mixtures (Moriarty III and Pieters, 2018). Based on the absence of apparent volcanic sources and the morphology of the deposits (e.g., hummocky terrain and viscous flow), the floor of the 73-km-wide Finsen crater plausibly represent impact-melt deposits. Finsen crater and the melt deposits were formed almost simultaneously in a single impact event, therefore, a flat and homogenous area, which is outlined on the floor of Finsen crater in Fig. 2, is selected as crater count area for CSFD measurements.

## 3. Methods

### 3.1. Crater identification

Craters are identified by their unique characteristics (e.g., presence of rim, circularity of the rim, etc.), and they are mapped by an almost evenly distributed three-point rim fitting method to eliminate any possible errors (Kneissl et al., 2011; Yue et al., 2019). The crater mapping work is done with an ArcGIS add-in "CraterTools", which automatically adjusts for map-projection distortions to prevent mismeasurement of crater diameters and count area (Kneissl et al., 2011). During the crater mapping, obvious secondary craters, which exhibit distinctive morphologies such as shallow, irregular shapes and occurrence in chains and clusters, sometimes with distinctive herring-bone patterns (e.g., McEwen and Bierhaus, 2006), are excluded to reduce contamination. In order to investigate the spatial distribution and variability of the mapped craters within the measurement area, two individual randomness analyses, standard deviation of adjacent area (SDAA) and mean 2nd-closest neighbor distance (M2CND), are performed in the widely used Craterstats software (Michael et al., 2012). Due to the inherent uncertainty in diameter measurements, which gets larger as craters approach the resolution limit, and the possibility that craters near the resolution limit will be missed, only craters with diameters larger than about 10 pixels of the basemap (here is 70 m) (Robbins et al., 2014; Wang et al., 2020) are kept for further AMA derivation. As a result, 216 craters with diameter larger than 70 m were kept and stored in a shapefile (locations are provided in supplementary material).

### 3.2. AMA derivation

The AMA of the outlined unit within the Finsen crater is derived using standard crater chronologies, which combines information from crater formation rates and radiometric ages of lunar rock samples. This method is widely used and well accepted to obtain AMAs of geological units on planetary bodies from remotely sensed data (e.g., Shoemaker et al., 1962; Baldwin, 1964; Hartmann, 1965; Arvidson et al., 1979; Neukum, 1983). After mapping craters on the outlined count area, the

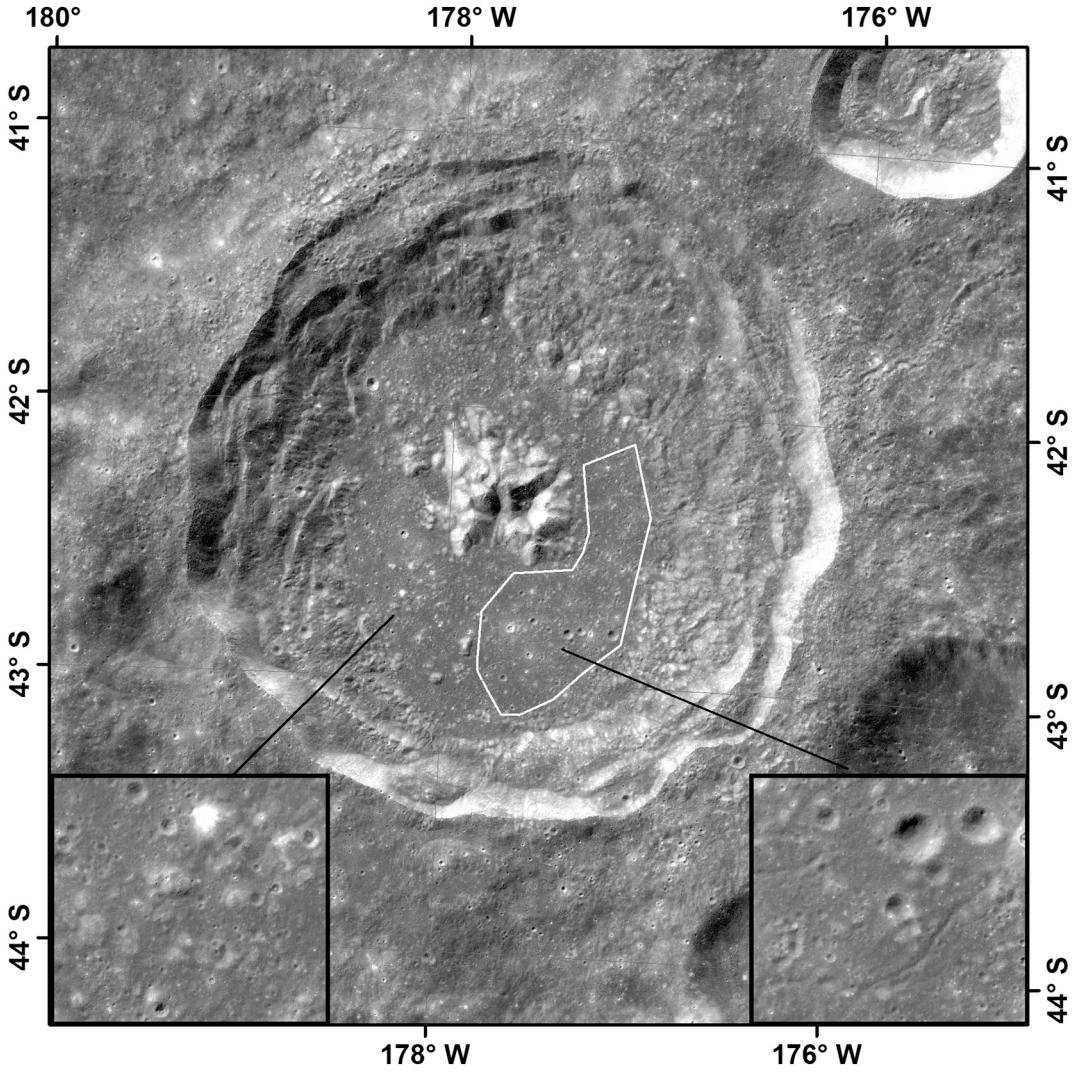


**Fig. 2.** Context map of Finsen crater (Chang'e-2 mosaic as base map), with crater count area being outlined in white polygon. The lower-left and lower-right insets show hummocky terrain and viscous flow, respectively.

obtained crater size-frequency distribution (CSFD) is plotted using pseudo-log binning with Craterstats (Michael and Neukum, 2010). The AMA of the area is derived by both cumulative and differential fit, with chronology function (CF) and production function (PF) from Neukum (1983).

### 3.3. Crater depth measurement

The depths of identified craters are calculated from the DEM by the profile-average-depth method (Vincent et al., 2014; Gou et al., 2018; Robbins et al., 2018). The major steps are described as follows. First, 8 profiles crossing the initial circle center of each crater are drawn starting from north at a fixed interval angle 22.5°. Second, each profile is updated by finding local topographic inflection point (local maxima). Third, the depth of the crater is calculated as the average elevation difference between the rim and the floor of each profile. More detail about crater depth measurement can be found in Gou et al. (2018).

## 4. Result and geologic implications

### 4.1. AMA of Finsen crater

Spatial randomness analysis of the mapped craters falls within ±3σ of the expectation value derived from Monte Carlo simulation for all the diameters (Fig. 3), indicating craters in the size range examined show a random spatial distribution. AMAs of Finsen crater derived from cumulative and differential fits, which are based on CSFD measurements on an representative area of impact-melt deposits on the floor of Finsen crater, are $3.47^{+0.067}_{-0.12}$Ga and $3.51^{+0.10}_{-0.39}$Ga, respectively (Fig. 3). These two AMAs are within each other's error bars, suggesting they are in excellent agreement that reveal an AMA of ~3.5 Ga. AMAs were also computed with the newer PF and CF values (Neukum et al., 2001) and found to produce the same model age, indicating the determined AMA (~3.5 Ga) is robust. This model age is consistent with the AMA ($3.61^{+0.02}_{-0.02}$Ga) derived by Ivanov et al. (2018), indicating Finsen crater is Imbrium-aged. The slight model age difference between this study and Ivanov et al. (2018) is probably due to factors such as the difference in count area selection and crater identification (Robbins et al., 2014). The derived AMA (~3.5 Ga) of Finsen crater is consistent with the geology context that ejecta from Finsen covers the southeastern and northeastern part of the interior floor of Leibnitz (~3.88 Ga) and Von Kármán (~3.97 Ga) crater, respectively (Stuart-Alexander, 1978; Yingst et al., 2017).

### 4.2. Regolith growth rate at Chang'e-4 landing site

Previous works suggested the Chang'e-4 landing site is chiefly covered by ejecta excavated by Finsen crater (e.g., Gou et al., 2019; Di et al., 2019b; Lin et al., 2020). The surface of the landing site has then been bombarded by meteorites for billions of years. Therefore, a fine-grained layer termed "regolith", which is mainly composed of unconsolidated materials, accumulated gradually by the continuous impacting and gardening of the lunar surface materials. The variations of permittivity with depth and the LPR radargrams indicate that the thickness of the Finsen crater ejecta-sourced fine-grained regolith at Chang'e-4 landing site is about 12 m (Lai et al., 2019; Li et al., 2020). Simplifying the actual dynamic regolith growth process, we assume the lunar regolith at Chang'e-4 landing site accumulated immediately and steadily after the formation of Finsen crater about 3.5 billion years ago, the average regolith growth rate at Chang'e-4 landing site is thus estimated to be about 3.4 m/Gyr (12 m/3.5 Ga).

The estimated average regolith growth rate at Chang'e-4 landing site is consistent with previous investigations that indicated a particularly

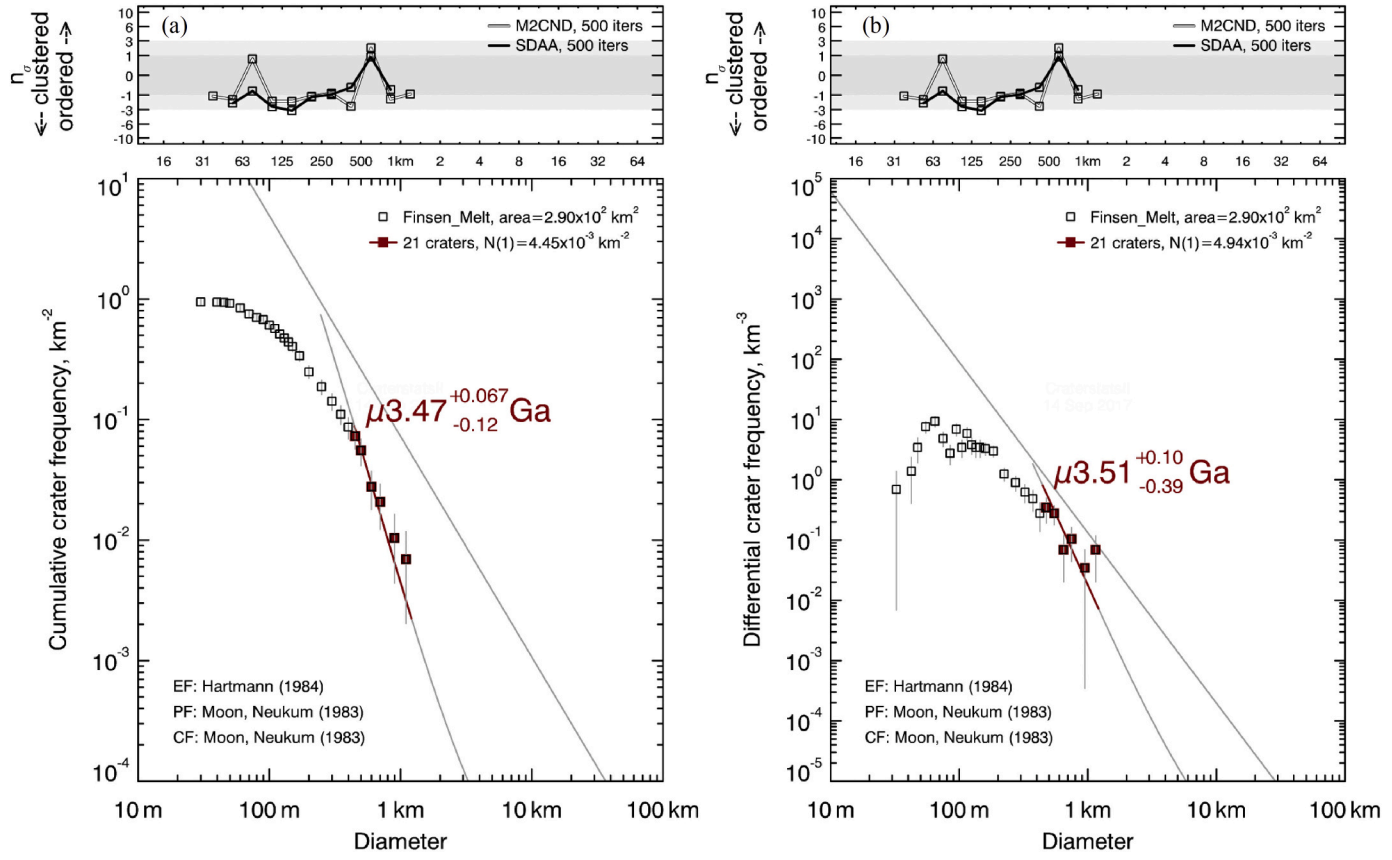


**Fig. 3.** AMA of Finsen crater derived by different fits: (a) cumulative fit, (b) differential fit. Craters for fitting are marked as red filled squares. (For interpretation of the references to colour in this figure legend, the reader is referred to the web version of this article).

high regolith formation rate of about 3–5 m/Gyr between ~3.5 and ~4.0 billion years ago, but it is rather faster than the very slow growth rate of about 1–1.5 m/Gyr from ~3.5 Ga to the present day (Oberbeck and Quaide, 1968; Quaide and Oberbeck, 1975; Hörz et al., 1991). Compared with Apollo landing sites of similar age (Table 1), the estimated regolith growth rate at the Chang'e-4 landing site is greater, except for Apollo 16. The relatively faster regolith growth rate at the Chang'e-4 landing site may be attributed to Finsen ejecta possibly having a low weathering resistivity that is easily weathered by harsh space environment. However, this rate is incomparable with rather rapid growth rate of new regolith (about 5–10 m/Gyr) at Chang'e-3 landing site (Table 1) that results from very fast space weathering for young fresh surfaces (~100 Ma) (Fa et al., 2015; Lai et al., 2016), indicating a great regional variation of regolith formation rate on the lunar surface.

### 4.3. Crater degradation/infilling rate within Finsen crater

Small craters are easily destroyed with time by erosion of crater rim/ejecta and infilling of crater interior by geologic processes (e.g., wall collapse and mass wasting) (e.g., Barlow, 2015). After 3 Gyr of evolution, a 300 m crater is almost imperceptible, while a 1 km crater still has significant relief (Fassett and Thomson, 2014). Therefore, variations of depth for craters within Finsen crater can provide constraints on the crater degradation/infilling rate on the lunar surface. The initial morphometry of fresh simple craters has been well-studied, with depth-to-diameter (d/D) ratio as a key parameter for describing/quantifying crater morphology. On the Moon, fresh, strength-regime dominated craters (diameters less than 400 m) exhibit d/D ratios of ~0.11, ~0.12, ~0.13, ~0.15, and ~0.17 (Stopar et al., 2017) due to varying crater shapes (flat floor, normal bowl, and central mound) and diameter bin examined (200–400 m, 100–200 m, and 40-100 m); whereas larger-scale craters (diameters 400 m–10 km) have d/D ratios averaging around 0.21 (Stopar et al., 2017).

The twenty-five largest craters within the count area, whose diameters range from 407 m to 1175 m (details are provided in supplementary material), are selected for average degradation/infilling rate estimation in this study. To simplify the analysis here, according to the scaling law (Melosh, 1989), the depth of a simple fresh crater is about 1/5 of its final diameter when it forms after the modification stage is complete. The original depths of the selected twenty-five largest craters within Finsen crater are estimated to range from 81 m to 235 m. Their current crater depths that are calculated by the above described profile-average-depth method vary from 4 m to 157 m (details are provided in supplementary material). Therefore, the differences between the estimated original depths and the calculated current depths, as well as the AMA of Finsen crater are used to estimate crater degradation/infilling rates. Results show that the average crater degradation/infilling rate within Finsen crater is about 21 ± 3 m/Gyr, which has the same order of magnitude to that on the lunar maria (about 32 m/Gyr) (Fassett and Thomson, 2014). The slight discrepancy of average degradation/infilling rates may be related to many potential factors, such as target material that affects resistance to degradation (impact melt inside Finsen crater vs. mare basalts for lunar maria) (Melosh, 1989), degradation time implied by the AMAs (~3.5 Ga for craters on the floor of Finsen crater vs. ~3 Ga for craters on lunar maria), and location that affects degradation intensity (inside Finsen crater vs. inside impact basin for lunar maria), etc. However, this estimated degradation/infilling rate is much slower than that on other airless rocky bodies. For example, average degradation/infilling rate on Vesta is 350 m/Gyr (Vincent et al., 2014), and on Gaspra is 100–1000 m/Gyr (Carr et al., 1994). One of the most likely reasons is that craters on asteroids are easily degraded or even erased by mass movements (e.g., landslides and crater erasures) caused by impact-induced seismic shaking (e.g., Carr et al., 1994; Richardson et al., 2004; Jutzi et al., 2013; Matsue et al., 2020).

**Table 1**
Summary of estimated average regolith growth rate.

| Missions | Regolith thickness*(m) | Age** (Ga) | Growth rate (m/Gyr) | References |
|---|---|---|---|---|
| Apollo 11 | 4.4 | 3.58 | 1.23 | (Nakamura et al., 1975; Stöffler and Ryder, 2001) |
| Apollo 12 | 3.7 | 3.15 | 1.17 | (Nakamura et al., 1975; Stöffler and Ryder, 2001) |
| Apollo 14 | 8.5 | 3.94 | 2.16 | (Cooper et al., 1974; Snape et al., 2016) |
| Apollo 15 | 4.4 | 3.30 | 1.33 | (Nakamura et al., 1975; Stöffler and Ryder, 2001) |
| Apollo 16 | 12.2 | 3.74 | 3.26 | (Cooper et al., 1974; Stöffler and Ryder, 2001) |
| Apollo 17 | 4 | 3.75 | 1.07 | (Cooper et al., 1974; Stöffler and Ryder, 2001) |
| Chang'e-3 | 0.95 | 0.1 | 5–10*** | (Fa et al., 2015; Lai et al., 2016) |
| Chang'e-4 | 12 | 3.5 | 3.4 | (Lai et al., 2019; Li et al., 2020) |

* The regolith thicknesses are in situ measured values.
** The ages for Apollo missions are absolute ages determined by radiometric dating, the ages for Chang'e-3/4 are AMAs determined from CSFD measurements.
*** This estimation combines an uncertainty of 30 Ma in age and 5% in depth.

## 5. Conclusion

As the primary source of materials measured inside of Von Kármán crater by the Chang'e-4 rover, the absolute model age (AMA) of Finsen crater is derived from the crater size-frequency distribution (CSFD) measurements in this study. Both cumulative and differential fits using the Neukum chronology (Neukum, 1983) reveal an AMA of ~3.5 Ga, indicating Finsen crater is Imbrium-aged.

Based on thickness estimation of the Finsen crater ejecta-sourced fine-grained regolith at Chang'e-4 landing site (~12 m) (Lai et al., 2019; Li et al., 2020), the average regolith growth rate at the landing site is estimated to be about 3.4 m/Gyr, which is consistent with previous investigations that indicated a particularly high regolith formation rate of about 3–5 m/Gyr between ~3.5 and ~4.0 billion years ago.

The current depths of 25 largest craters on the floor of Finsen crater are calculated by the profile-average-depth method, and their original depths are estimated under the assumption that the initial depth-to-diameter (d/D) ratio is 0.2. Differences between the estimated original depths and the calculated current average depths, as well as the AMA of Finsen crater indicate the average crater degradation/infilling rate within Finsen crater is about 21 ± 3 m/Gyr, which has the same order of magnitude to that on the lunar maria (about 32 m/Gyr).

## Declaration of Competing Interest

The authors declare that they have no known competing financial interests or personal relationships that could have appeared to influence the work reported in this article.

## Acknowledgements

This work was supported by the Strategic Priority Research Program of Chinese Academy of Sciences (grant No. XDB41000000), National Natural Science Foundation of China (grant Nos. 41702354 and 41941003), Macao Young Scholars Program (grant No. AM201902), and Science and Technology Development Fund of Macau (grant No. 131/2017/A3). The authors thank Jun Du for discussions about crater degradation process, and greatly appreciate Mikhail Ivanov and

Michelle Kirchoff for constructive reviews that improved the manuscript quality substantially.

## Appendix A. Supplementary data

Supplementary data to this article can be found online at https://doi.org/10.1016/j.icarus.2020.114046.

## References


Arvidson, R.E., Boyce, J., Chapman, C., Cintala, M., Fulchignoni, M., Moore, H., Neukum, G., Schultz, P., Soderblom, L., Strom, R., Woronow, A., Young, R., 1979. Standard techniques for presentation and analysis of crater size-frequency data. Icarus. 37 (2), 467–474.

Baldwin, R.B., 1964. Lunar crater counts. Astron. J. 69, 377.

Barlow, N.G., 2015. Constraining geologic properties and processes through the use of impact craters. Geomorphology. 240, 18–33.

Carr, M.H., Kirk, R.L., Mcewen, A.S., Veverka, J., Thomas, P., Head, J.W., Murchie, S.L., 1994. The geology of Gaspra. Icarus. 107 (1), 61–71.

Cooper, M.R., Kovach, R.L., Watkins, J.S., 1974. Lunar near-surface structure. Rev. Geophys. 12 (3), 291–308.

Di, K., Liu, Z., Liu, B., Wan, W., Peng, M., Wang, Y., Gou, S., Yue, Z., Xn, X., Jia, M., Niu, S., 2019a. Chang'e-4 lander localization based on multi-source data. J. Remote Sens. 23 (1), 177–184.

Di, K., Zhu, M.-H., Yue, Z., Lin, Y., Wan, W., Liu, Zhaoqin, Gou, S., Liu, B., Peng, Man, Wang, Y., Niu, S., Zhang, J., Li, J., Xie, J., Xi, L., Yang, J., Xue, B., 2019b. Topographic evolution of Von Kármán crater revealed by the lunar rover Yutu-2. Geophys. Res. Lett. 46 (22), 12764–12770.

Fa, W., Zhu, M.-H., Liu, T., Plescia, J.B., 2015. Regolith stratigraphy at the Chang'E-3 landing site as seen by lunar penetrating radar. Geophys. Res. Lett. 42 (23), 10179–10187.

Fassett, C.I., Thomson, B.J., 2014. Crater degradation on the lunar maria: topographic diffusion and the rate of erosion on the moon. J. Geophys. Res: Planet. 119 (10), 2255–2271.

Fortezzo, C.M., Spudis, P.D., Harrel, S.L., 2020. Release of the Digital Unified Global Geologic Map of the Moon At 1:5,000,000- Scale. In: 51st Lunar and Planetary Science Conference, p. 2760 the Woodlands, Texas.

Gou, S., Yue, Z.Y., Di, K.C., Liu, Z.Q., 2018. A global catalogue of Ceres impact craters ≥ 1 km and preliminary analysis. Icarus. 302, 296–307.

Gou, S., Di, K., Yue, Z., Liu, Z., He, Z., Xu, R., Lin, H., Liu, B., Peng, M., Wan, W., Wang, Y., Liu, J., 2019. Lunar deep materials observed by Chang'e-4 rover. Earth Planet. Sci. Lett. 528, 115829.

Gou, S., Yue, Z., Di, K., Wan, W., Liu, Z., Liu, B., Peng, M., Wang, Y., He, Z., Xu, R., 2020a. In situ spectral measurements of space weathering by Chang'e-4 rover. Earth Planet. Sci. Lett. 535, 116117.

Gou, S., Di, K., Yue, Z., Liu, Z., He, Z., Xu, R., Liu, B., Peng, M., Wan, W., Wang, Y., Liu, J., 2020b. Forsteritic olivine and magnesium-rich orthopyroxene materials measured by Chang'e-4 rover. Icarus. 345, 113776.

Gou, S., Yue, Z., Di, K., Wang, J., Wan, W., Liu, Z., Liu, B., Peng, M., Wang, Y., He, Z., Xu, R., 2020c. Impact melt breccia and surrounding regolith measured by Chang'e-4 rover. Earth Planet. Sci. Lett. 544, 116378.

Hartmann, W.K., 1965. Terrestrial and lunar flux of large meteorites in the last two billion years. Icarus. 4 (2), 157–165.

Hörz, F., Grieve, R.A.F., Heiken, G., Spudis, P.D., Binder, A.B., 1991. Lunar surface processes. In: Heiken, G., Vaniman, D., French, B.M. (Eds.), Lunar Sourcebook. Cambridge University Press, New York, pp. 61–120.

Ivanov, M.A., Hiesinger, H., van der Bogert, C.H., Orgel, C., Pasckert, J.H., Head, J.W., 2018. Geologic history of the northern portion of the south pole-Aitken Basin on the moon. J. Geophys. Res: Planet. 123 (10), 2585–2612.

Jia, Y., Zou, Y., Ping, J., Xue, C., Yan, J., Ning, Y., 2018. The scientific objectives and payloads of Chang'E−4 mission. Planet. Space Sci. 162, 207–215.

Jutzi, M., Thomas, N., Benz, W., El Maarry, M.R., Jorda, L., Kührt, E., Preusker, F., 2013. The influence of recent major crater impacts on the surrounding surfaces of (21) Lutetia. Icarus. 226 (1), 89–100.

Kneissl, T., Van Gasselt, S., Neukum, G., 2011. Map-projection-independent crater size-frequency determination in GIS environments—new software tool for ArcGIS. Planet. Space Sci. 59 (11), 1243–1254.

Lai, J., Xu, Y., Zhang, X., Tang, Z., 2016. Structural analysis of lunar subsurface with Chang'E-3 lunar penetrating radar. Planet. Space Sci. 120, 96–102.

Lai, J., Xu, Y., Zhang, X., Xiao, L., Yan, Q., Meng, X., Zhou, B., Dong, Z., Zhao, D., 2019. Comparison of dielectric properties and structure of lunar regolith at chang'e-3 and chang'e-4 landing sites revealed by ground penetrating radar. Geophys. Res. Lett. 46, 12783–12793.

Li, C., Su, Y., Pettinelli, E., Xing, S., Ding, C., Liu, J., Ren, X., Lauro, S.E., Soldovieri, F., Zeng, X., Gao, X., Chen, W., Dai, S., Liu, D., Zhang, G., Zuo, W., Wen, W., Zhang, Z., Zhang, X., Zhang, H., 2020. The Moon's farside shallow subsurface structure unveiled by Chang'E-4 lunar penetrating radar. Sci. Adv. 6 (9), eaay6898.

Lin, H., He, Z., Yang, W., Lin, Y., Xu, R., Zhang, C., Zhu, M.-H., Chang, R., Zhang, J., Li, C., Lin, H., Liu, Y., Gou, S., Wei, Y., Hu, S., Xue, C., Yang, J., Zhong, J., Fu, X., Wan, W., Zou, Y., 2020. Olivine-norite rock detected by the lunar rover Yutu-2 likely crystallized from the SPA impact melt pool. Natl. Sci. Rev. 7, 913–920.

Matsue, K., Yasui, M., Arakawa, M., Hasegawa, S., 2020. Measurements of seismic waves induced by high-velocity impacts: implications for seismic shaking surrounding impact craters on asteroids. Icarus. 338, 113520.

McEwen, A.S., Bierhaus, E.B., 2006. The importance of secondary cratering to age constraints on planetary surfaces. Annu. Rev. Earth Planet. Sci. 34 (1), 535–567.

Melosh, H.J., 1989. Impact Cratering: A Geologic Process. Oxford University Press, New York.

Michael, G.G., Neukum, G., 2010. Planetary surface dating from crater size–frequency distribution measurements: partial resurfacing events and statistical age uncertainty. Earth Planet. Sci. Lett. 294 (3), 223–229.

Michael, G.G., Platz, T., Kneissl, T., Schmedemann, N., 2012. Planetary surface dating from crater size–frequency distribution measurements: spatial randomness and clustering. Icarus. 218 (1), 169–177.

Moriarty III, D.P., Pieters, C.M., 2018. The character of south pole-Aitken Basin: patterns of surface and subsurface composition. J. Geophys. Res: Planet. 123 (3), 729–747.

Moriarty, D.P., Pieters, C.M., Nettles, J., Isaacson, P.J., Cheek, L., Head, J.W., Tompkins, S., Petro, N., 2011. Finsen and Alder: A Compositional Study of Lunar Central Peak Craters in the South Pole-Aitken Basin. In: 42nd Lunar and Planetary Science Conference, p. 2564. The Woodlands, Texas.

Nakamura, Y., Dorman, J., Duennebier, F., Lammlein, D., Latham, G., 1975. Shallow lunar structure determined from the passive seismic experiment. Moon. 13 (1), 57–66.

Neukum, G., 1983. Meteoriten bombardement und Datierung planetarer Oberflächen (German original). Habilitation Dissertation for Faculty Membership. University of Munich.

Neukum, G., Ivanov, B.A., Hartmann, W.K., 2001. Cratering records in the inner solar system in relation to the lunar reference system. Space Sci. Rev. 96, 55–86.

Oberbeck, V.R., Quaide, W.L., 1968. Genetic implications of lunar regolith thickness variations. Icarus. 9 (1), 446–465.

Quaide, W., Oberbeck, V., 1975. Development of the mare regolith: some model considerations. Moon 13 (1), 27–55.

Ren, X., Liu, J.J., Wang, F.F., Wang, W.R., Mu, L.L., Li, H.H., 2014. A new lunar global topographic map products from Chang'E-2 stereo camera image data. In: European Planetary Science Congress. Centro de Congressos do Estoril, Cascais, Portugal. pp. EPSC2014-344.

Richardson, J.E., Melosh, H.J., Greenberg, R., 2004. Impact-induced seismic activity on asteroid 433 Eros: a surface modification process. Science. 306 (5701), 1526–1529.

Robbins, S.J., Antonenko, I., Kirchoff, M.R., Chapman, C.R., Fassett, C.I., Herrick, R.R., Singer, K., Zanetti, M., Lehan, C., Huang, D., Gay, P.L., 2014. The variability of crater identification among expert and community crater analysts. Icarus. 234, 109–131.

Robbins, S.J., Watters, W.A., Chappelow, J.E., Bray, V.J., Daubar, I.J., Craddock, R.A., Beyer, R.A., Landis, M., Ostrach, L.R., Tornabene, L., Riggs, J.D., Weaver, B.P., 2018. Measuring impact crater depth throughout the solar system. Meteorit. Planet. Sci. 53 (4), 583–637.

Shoemaker, E.M., Hackman, R.J., Eggleton, R.E., 1962. Interplanetary correlation of geologic time. Adv. Astronaut. Sci. 8, 70–79.

Smith, D.E., Zuber, M.T., Neumann, G.A., Lemoine, F.G., Mazarico, E., Torrence, M.H., McGarry, J.F., Rowlands, D.D., Head III, J.W., Duxbury, T.H., Aharonson, O., Lucey, P.G., Robinson, M.S., Barnouin, O.S., Cavanaugh, J.F., Sun, X., Liiva, P., Mao, D.-d., Smith, J.C., Bartels, A.E., 2010. Initial observations from the lunar orbiter laser altimeter (LOLA). Geophys. Res. Lett. 37 (18), L18204.

Snape, J.F., Nemchin, A.A., Grange, M.L., Bellucci, J.J., Thiessen, F., Whitehouse, M.J., 2016. Phosphate ages in Apollo 14 breccias: resolving multiple impact events with high precision U–Pb SIMS analyses. Geochim. Cosmochim. Acta 174, 13–29.

Stöffler, D., Ryder, G., 2001. Stratigraphy and isotope ages of lunar geologic units: chronological standard for the inner solar system. Space Sci. Rev. 96 (1), 9–54.

Stopar, J.D., Robinson, M.S., Barnouin, O.S., McEwen, A.S., Speyerer, E.J., Henriksen, M. R., Sutton, S.S., 2017. Relative depths of simple craters and the nature of the lunar regolith. Icarus. 298, 34–48.

Stuart-Alexander, D.E., 1978. Geologic map of the central far side of the Moon. http://pubs.er.usgs.gov/publication/i1047.

Vincent, J.-B., Schenk, P., Nathues, A., 2014. Crater depth-to-diameter distribution and surface properties of (4) vesta. Planet. Space Sci. 103, 57–65.

Wang, Y., Xie, M., Xiao, Z., Cui, J., 2020. The minimum confidence limit for diameters in crater counts. Icarus. 341, 113645.

Yingst, R.A., Chuang, F.C., Berman, D.C., Mest, S.C., 2017. Geologic Mapping of the Planck Quadrangle of the Moon (LQ-29). In: 48th Lunar and Planetary Science Conference, p. 1680 the Woodlands, Texas.

Yue, Z., Di, K., Liu, Z., Michael, G., Jia, M., Xin, X., Liu, B., Peng, M., Liu, J., 2019. Lunar regolith thickness deduced from concentric craters in the CE-5 landing area. Icarus. 329, 46–54.

Zhao, B., Yang, J., Wen, D., Gao, W., Chang, L., Song, Z., Xue, B., Zhao, W., 2011. Overall scheme and on-orbit images of Chang'E-2 lunar satellite CCD stereo camera. Sci. China Technol. Sci. 54 (9), 2237.